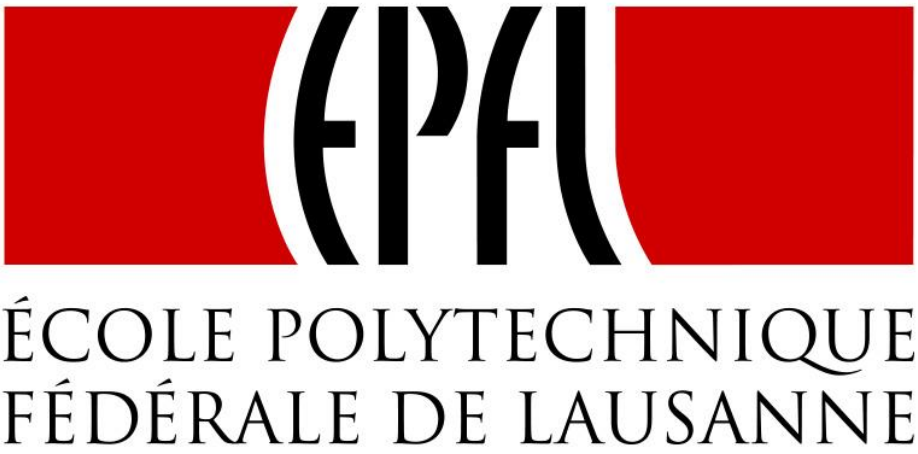

ENTRAINMENT PROPERTIES OF EXPLICIT AND GENERIC MODELS OF THE CIRCADIAN OSCILLATOR

Project report by Esther LECOMPTE and Souhail ELAISSAOUI

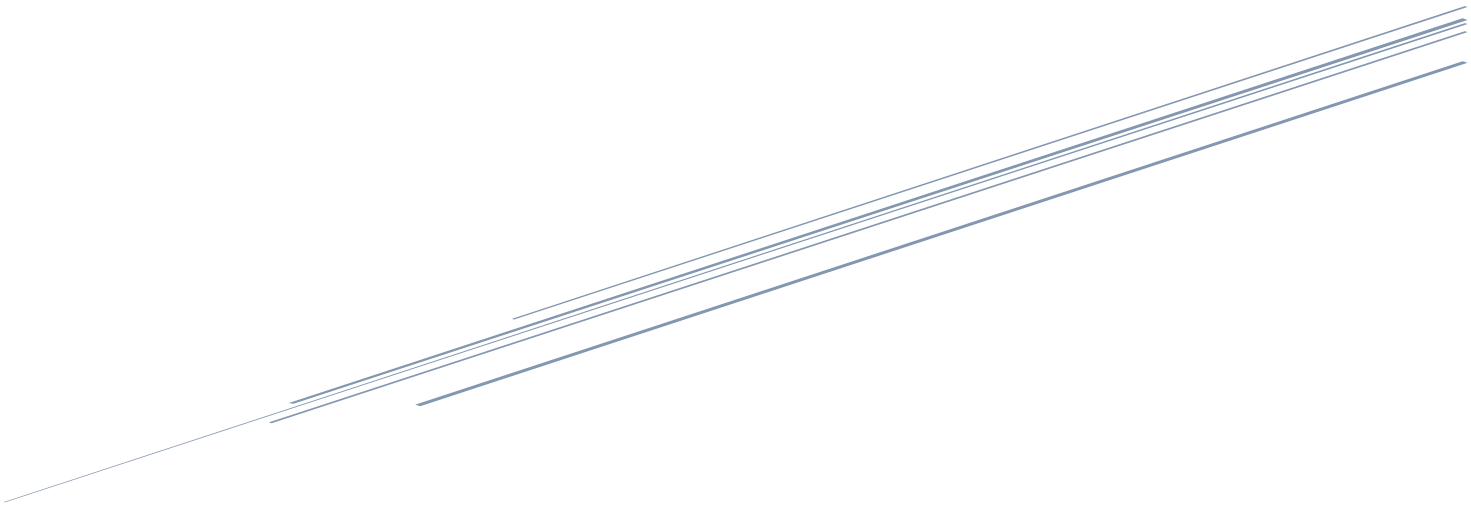

December 2017, Professor: Felix Naef
BIO341-Modélisation mathématique et computationnelle en biologie

Introduction

From conception to death, life encompasses innumerable processes in continuous change and for most of them, repetitively. Life on earth has to cope with a highly cyclic environment and over time, evolution has driven mammals to adapt to their environment. Therefore, cyclic phenomena are found in all living organisms and at all levels of organization.

Many physiological and behavioural parameters are influenced by daily cyclic variations such as the external light-dark cycle. For instance, blood pressure, heart rate, body temperature, or sleep-wake cycles change considerably during the course of a day.

The central circadian (Latin: "about one day") clock, which governs the 24 hours-rhythms, is located in the suprachiasmatic nuclei (SCN) of the ventral hypothalamus.

In general, a circadian clock, or circadian oscillator, is a biochemical oscillator that cycles with a stable phase and is synchronized with solar time.

Such a clock in vivo has a period close to 24 hours (the earth solar day). In most living things, internally synchronized circadian clocks make it possible for the organism to anticipate daily environmental changes corresponding to the day–night cycle and adjust its biology and behaviour accordingly.

There are also other external secondary cycles or periodic events such as food availability and biological or social signals.

In this report, the dynamics of an oscillator entrained by an external stimulus will be studied as a simplified model of the circadian clock.

Through a mathematic modelling software and theoretical notions, the behaviour of this model will be analysed.

A three-variable model has been chosen in order to implement the negative feedback loop oscillator. Then, a generic 2D model of biological oscillators will be introduced, that is valid near the onset of a stable limit cycle, called in dynamical systems a supercritical Hopf bifurcation.

A. A three-variable model for circadian oscillations in single cells

The model

A three-variable model for circadian oscillation in single cells is considered: X, the clock gene mRNA, produces a clock protein, Y, which in turn, activates Z, a transcriptional inhibitor. A sketch of the model is represented in Figure 1. Each variable has a growth rate (first term) and a decrease rate (second term). The equations of the model are the following:

$$\frac{dX}{dt} = v_1 \times \frac{{K_1}^4}{{K_1}^4 + Z^4} - v_2 \times \frac{X}{K_2 + X}$$

$$\frac{dY}{dt} = K_3 \times X - v_4 \times \frac{Y}{K_4 + Y}$$

$$\frac{dZ}{dt} = K_5 \times Y - v_6 \times \frac{Z}{K_6 + Z}$$

v_1 is the maximum transcription rate, v_2 is the saturation value of the decrease rate of X. v_4 is the saturation value of the decrease rate of Y. v_6 is the saturation value of the decrease rate of Z.

K_1, K_2, K_4 and K_6, are respectively the Z, X, Y and Z quantities where the X growth rate, the X decrease rate, the Y decrease rate and the Z decrease rate, are at half their maximum.

K_3 and K_5 are respectively the relative growth rate of Y in function of X and Z in function of Y.

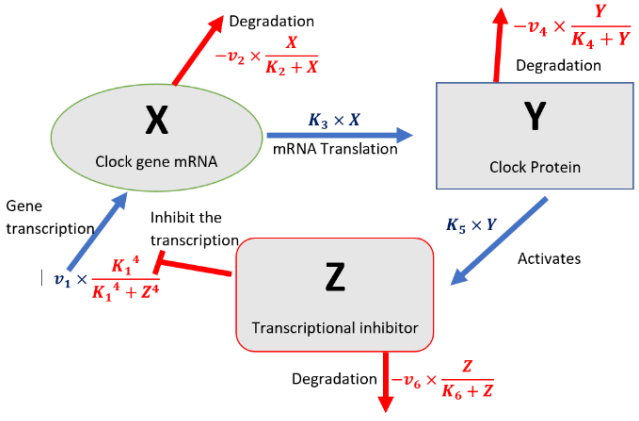

Figure 1 - Sketch of the model

These variables could represent the PER clock gene mRNA (X): when PER protein (Y) levels increase, the inhibition of PER transcription increases, lowering the protein levels. However, because PER protein cannot directly bind to DNA, it does not directly

influence its own transcription; alternatively, it inhibits its own activators (Z).

This The previous model is a simplified model of a circadian oscillator in single cells, taking into account some basic ingredients, notably the negative feedback loop. A clock gene mRNA (X) produces a clock protein (Y) which, in turn, activates a transcriptional inhibitor (Z). In a negative feedback loop, each reaction includes many different processes and it can hardly be linear: the mRNA transcription, for example, involves the fact that the mRNA crosses the nucleus membrane, binds to the ribosome, and then starts the translation with very complex processes that are clearly not linear. The inhibitor activation could also involve binding of different proteins and cofactors, this can involve a certain delay and can hardly be linear. This delay would not be considered in the system.

Moreover, the degradation rates of the components are modelized with Michaelis Menten kinetics, which is assumed to be an accurate approximation for biochemical reactions involving a single substrate. However, the number of substrates involved in each degradation reactions can not be confirmed for this model. Finally, the presented model is described in continuous time whereas the biological system would rather correspond to a discrete time system meaning that there are specific time moments at which the events occur.

For these reasons, the assumptions of the model can be criticized, but this simplified model allows to give an overview to represent the phenomena.

Simulation of the model

To gain intuition about the model, a single cell oscillator was considered without any further coupling/interaction with the environment. In order to obtain a correct behaviour, appropriate initial conditions and time integration parameters were set.

Using MATLAB®, a representative trajectory was plotted in 2D and 3D in Figure 2 using $(X_0, Y_0, Z_0) =$ (0, 1, 5) as initial condition.

Oscillations can be seen for each component. The amplitude of the signal stabilizes after approximately 10 days. The transient time varies depending on the initial conditions. Moreover, a period value, near 1 day, can be noticed.

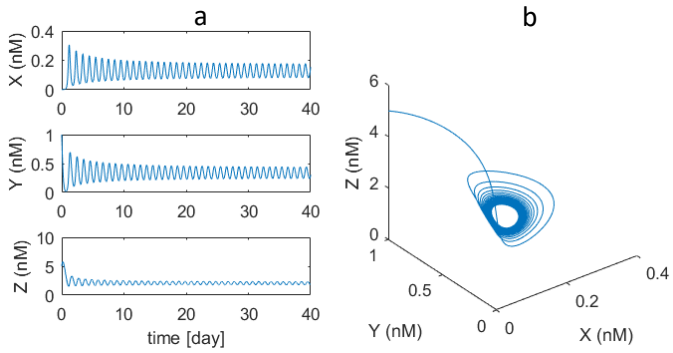

Figure 2

a. Oscillations of each component in function of time, the values used were: $v_1 = 0.7nMh$; $v_2 = v_4 = v_6 = 0{,}35nMh^{-1}$; $K_1 = K_2 = K_4 = K_6 = 1Nm$; $K_3 = K_5 = 0.7\ h^{-1}$; dt = 0.1h. Initial conditions are (0, 1, 5).

b. 3D representation of the trajectories, the limit cycle is appearing for large times.

To calculate accurately the period of the model, a Fourier analysis was used on a long trajectory as shown in Figure 3. The calculated period is 23.57 hours, which corresponds approximately to the 24 hours, external period of a circadian oscillator.

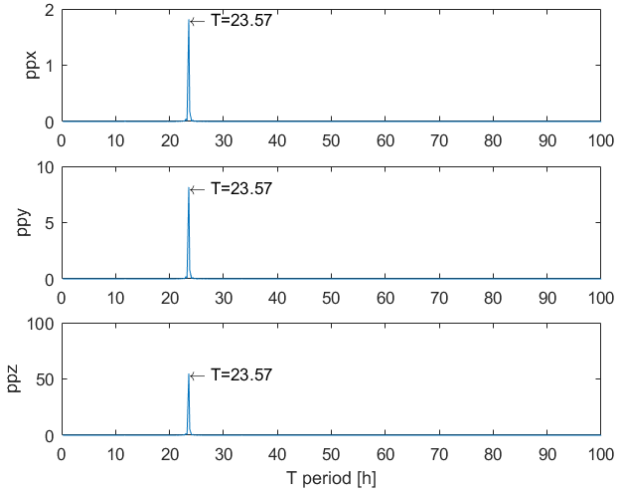

Figure 3 - Oscillation periods found with a Fourier analysis, the same period, T = 23.57 h, was calculated for the three variables. This period corresponds approximately to one day, as it is expected for a circadian oscillator.

Taking v_1, the transcription rate, as the variant bifurcation parameter, different trajectories of the model are plotted in Figure 4. The limit cycle only appears for certain values of v_1. For small values ($v_1 = 0.01$ or $v_1 = 0.1$) or high values ($v_1 = 5$), the

trajectory converges towards a point while for $v_1 = 1.5$, the trajectory forms a limit cycle.

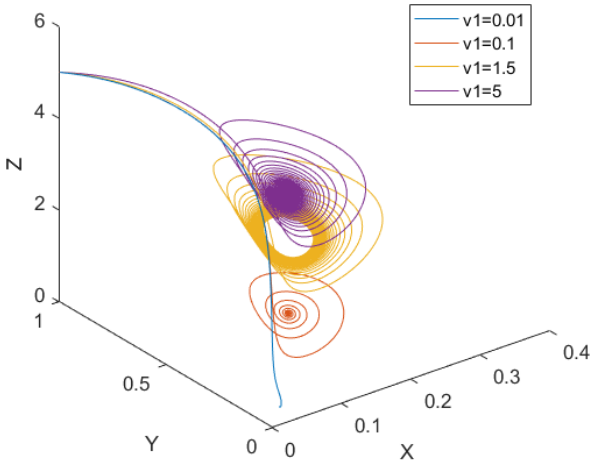

Figure 4 - Different trajectories in function of v_1. If v_1 is high, the trajectories converge also higher in the z-axis. A limit cycle is observable for $v_1 = 1.5$. For other values, the trajectories converge to a point.

In order to study the presence of a limit cycle in function of the bifurcation parameter v_1, a bifurcation diagram of the model is represented in Figure 5. A limit cycle can be seen in the diagram, starting from $v_1 \approx 0.3$ nM/h. The onset of a limit cycle is called a "supercritical Hopf bifurcation". Above this value, the radius of this limit cycle increases with v_1 until v_1 equals approximately 1 nM/h, where the radius of the limit cycle is at its maximum. Then the radius decreases until disappearing around $v_1 \approx 4$ nM/h.

It can also be noticed that the value of X, the clock gene mRNA, converges toward a limit value of 0.14 nM when v_1 increases.
For a period that best approximates the 24 hours of a day, the optimal v_1 value is deduced from Figure 5b and should be around 0.9 nM/h, which corresponds to the point where the limit cycle radius is near to its maximum.

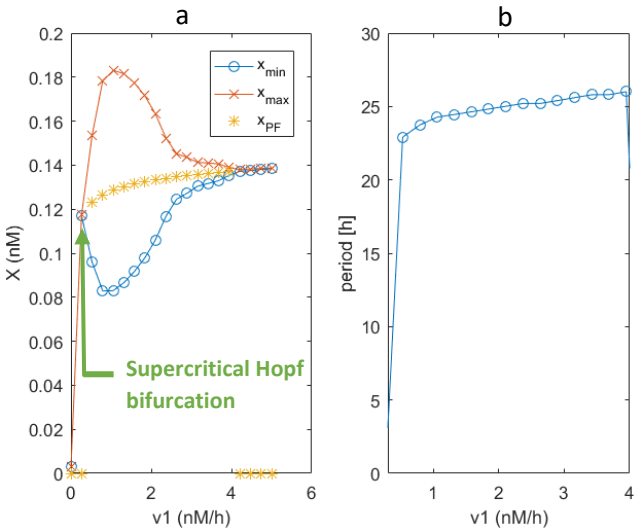

Figure 5 - a. Bifurcation diagram for the model, the transcription rate v_1 varies in the interval]0, 5] nMh-1. The onset of a limit cycle is called a "supercritical Hopf bifurcation". The x-coordinate of the unstable fixed point is represented in yellow.
b. Evolution of the oscillator's period in function of v_1 where v_1 varies in the interval [0.3, 4].
There is a minimum value of v_1 (0.3nM/h) in order to have a non-zero period. For a period that best approximates the 24 hours of a day, the optimal v_1 value should be around 0.9 nM/h.

For a fixed value of the transcription rate ($v_1 = 0.5$ nM/h), the system has one unstable fixed point:

$$\mathrm{x_0} = (0.1228, \quad 0.3254, \quad 1.8637)$$

The Jacobian matrix is calculated around this fixed point and the eigenvalues are:

$$\lambda_1 = -0.5202$$
$$\lambda_2 = 0.0003 + 0.2757\mathrm{i}$$
$$\lambda_3 = 0.0003 - 0.2757\mathrm{i}$$

The associated eigenvectors are:

$$\mathbf{v_1} = (-0.2501, \quad 0.5456, \quad -0.7998)$$

$$\mathbf{v_2} = (-0.1258 + 0.1247\mathrm{i}, \quad 0.0561 + 0.36\mathrm{i}, \quad 0.9143)$$

$$\mathbf{v_3} = (-0.1258 - 0.1247\mathrm{i}, \quad 0.0561 - 0.36\mathrm{i}, \quad 0.9143)$$

Taking **V** as the eigenvectors matrix, the trajectory can be expressed in the eigenvector basis through a coefficient vector, $\mathbf{c} = (c_1, c_2, c_3)$.

$$\mathbf{V} = \begin{pmatrix} \mathrm{v_{1x}} & \mathrm{v_{1y}} & \mathrm{v_{1z}} \\ \mathrm{v_{2x}} & \mathrm{v_{2y}} & \mathrm{v_{2z}} \\ \mathrm{v_{3x}} & \mathrm{v_{3y}} & \mathrm{v_{3z}} \end{pmatrix}$$

$$\begin{pmatrix} \Delta X \\ \Delta Y \\ \Delta Z \end{pmatrix} = \begin{pmatrix} X - \dot{X} \\ Y - \dot{Y} \\ Z - \dot{Z} \end{pmatrix} = \mathbf{c} \times \mathbf{V}$$

with $\dot{X}, \dot{Y}$ and $\dot{Z}$ corresponding to the coordinates of the fixed point.

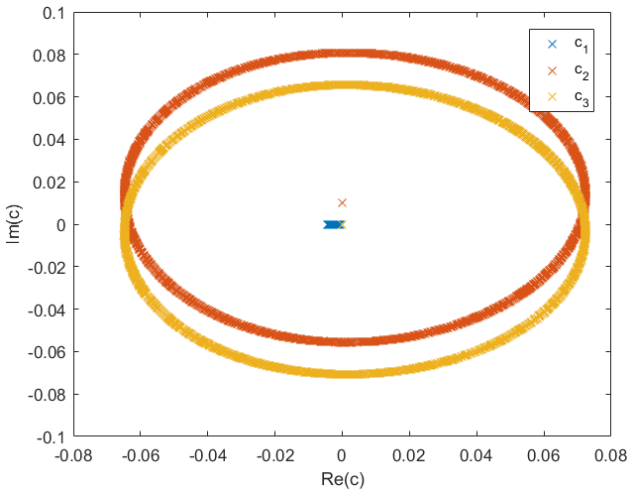

Figure 6 – Representation of the real and imaginary parts of the coefficients when expressing the trajectory in the eigenvector basis.

It can be seen that c_1 vary very slightly compared to c_2 and c_3, as all its values are real, with a zero imaginary part. The two other variables, c_2 and c_3 vary highly more and have an important imaginary part. Therefore, the first eigenvector, $\mathbf{v_1}$, can be neglected compared to $\mathbf{v_2}$ and $\mathbf{v_3}$. With these two eigenvectors, the trajectory can be expressed in a 2D plane.

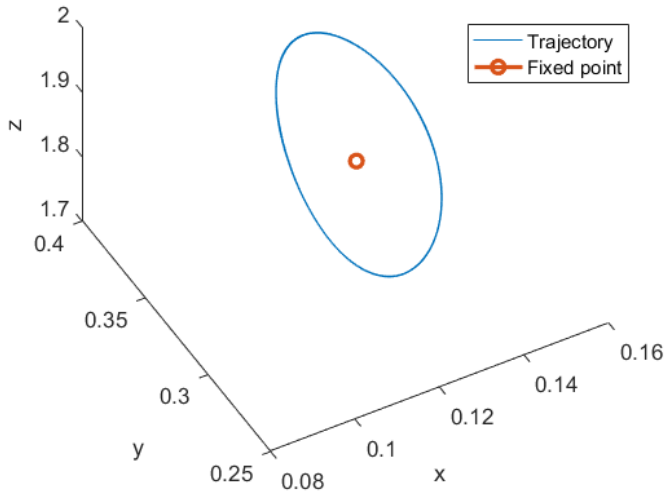

Figure 7- Zoom on the trajectory near the bifurcation, the limit cycle near the bifurcation occurs mostly in a 2D-plane

The fact that there are only 2 components that are highly variable can be confirmed in a zoomed representation of the trajectory as shown in Figure 7. Indeed, the limit cycle occurs mostly in a 2D-plane.

B. Generic model of a limit cycle oscillator: Supercritical Hopf oscillators

The following sections of the report focus on a generic model in 2D of a nonlinear oscillator near a supercritical Hopf bifurcation. This latter corresponds to the onset of a stable limit cycle. The following model is a good approximation in the 2D plane of the limit cycle and is described in complex notation ($z = x + iy$ and $|z| = \sqrt{x^2 + y^2}$) as:

$$\dot{z} = (\mu + i\omega)z - (g + ih)z|z|^2 \qquad (1)$$

With $\omega > 0$ the intrinsic frequency ($2\pi/T$) of the oscillator and $\mu, g > 0$ and h are parameters of the oscillator which depend on the microscopic details (chemical rates, etc).

The model (1) can be written in cartesian coordinates considering $\dot{z} = \dot{x} + i\dot{y}$:

$$\begin{cases} \dot{x} = \mu x - \omega y - (gx - hy)(x^2 + y^2) \\ \dot{y} = \omega x + \mu y - (gy - hx)(x^2 + y^2) \end{cases}$$

Additionally, it is also possible to write the model in polar coordinates using the change of variable $z(t) = R(t)e^{i\varphi(t)}$:

$$\begin{cases} \dot{R} = \mu R - gR^3 \\ \dot{\varphi} = \omega - hR^2 \end{cases}$$

With $R(t)$ the radial and $\varphi(t)$ the angular coordinates of the complex variable $z(t)$.

We observe that the parameter h links the phase variations with the radius of the variable $z(t)$. In Figure 5a, one observes that, near the supercritical Hopf bifurcation, the radius of the limit cycle, deduced from the difference between x_{max} and x_{min}, grows as v_1 becomes higher. And in Figure 5b, higher values of v_1 correspond to larger periods and thus slower phase speeds. Therefore, we can deduce that the parameter h should be positive.

The model (1) shows a limit cycle in the x, y-plane under the condition that the radius of $z(t)$ is constant, that is $\dot{R} = 0$, which leads a non-zero and positive radius of the limit cycle (μ and g being positive):

$$R = \sqrt{\mu/g} \qquad (2)$$

Under this condition, the relationship on the phase becomes: $\dot{\varphi} = \omega - \frac{h\mu}{g}$ and is positive for $\omega > \frac{h\mu}{g}$.

C. Entrainment of a Hopf oscillators

Considering that the previous oscillator (1) is entrained by an external periodic signal, the model can be described as:

$$\dot{z} = (\mu + i\omega)z - (g + ih)z|z|^2 + Fe^{i\Omega t}$$

Where $F > 0$ and $\Omega = \frac{2\pi}{T}$ is the external frequency.

This model contains an explicit time dependence $e^{i\Omega t}$ and implies a shift in the oscillation due to the external signal.

One characteristic of circadian oscillators consists in the fact that if a perturbation is applied, the system will return to its limit cycle with a fixed period and amplitude.

Eliminate the time-dependence

In order to make the previous dynamical system autonomous (no dependence in time), the following change variable is applied, corresponding to a base change in a rotating base at the frequency of the external stimulus:

$$Z(t) = z(t)e^{-i\Omega t}$$

By introducing the angular frequency difference $\Delta = \omega - \Omega$, an equation for $\dot{Z}$ is obtained:

$$\dot{Z} = \mu Z + i\Delta Z - (g + ih)Z|Z|^2 + F \qquad (3)$$

The model (3) can be written in cartesian coordinates considering $\dot{Z} = \dot{X} + i\dot{Y}$:

$$\begin{cases} \dot{X} = \mu X - \Delta Y - (gX - hY)(X^2 + Y^2) + F \\ \dot{Y} = \Delta X + \mu Y - (gY - hX)(X^2 + Y^2) \end{cases}$$

In polar coordinates, the system becomes:

$$\begin{cases} \dot{R} = \mu R - gR^3 + Fcos\theta \\ \dot{\theta} = \Delta - hR^2 - \frac{F}{R}sin\theta \end{cases} \qquad (4)$$

Establish the phase portrait for the entrained model

The conditions under which the oscillator is synchronized by the external stimulus F, will now be analysed. We talk about synchronization when the system (3) owns a stable fixed point or a stable spiral. Indeed, a fixed point or a spiral gives information both on the amplitude of the entrained system and on the phase difference between the two oscillators. Hence, when a stable fixed point or a stable spiral is present in the system, this latter converges to it such that the difference in phases between the two oscillators tends to a constant. This is called phase locking or synchronisation.

In this section, the phase portraits of the system are plotted for different sets of variables (Δ, F, μ). The fixed points are the intersections of the isoclines, that is $\dot{X} = 0$ (iso-x) and $\dot{Y} = 0$ (iso-y) and are numerically obtained by solving $\dot{R} = 0$ and $\dot{\theta} = 0$ that is:

$$\begin{cases} Fcos\theta = -\mu R + gR^3 \\ Fsin\theta = \Delta R - hR^3 \end{cases} \qquad (5)$$

which leads to the following expression:

$$(gR^3 - \mu R)^2 + (\Delta R - hR^3)^2 - F^2 = 0$$

$$(g^2 + h^2)R^6 - 2(g\mu + h\Delta)R^4 + (\mu^2 + \Delta^2)R^2 - F^2 = 0$$

There are thus a maximum of 3 positive radius.

The stability of the fixed points is evaluated by considering the eigenvalues of the Jacobian at the fixed points:

$$J(x,y) = \begin{pmatrix} \mu - 3gX^2 - gY^2 + 2hXY & -\Delta - 2gXY + hX^2 + 3hY^2 \\ \Delta - 2gXY - 3hX^2 - hY^2 & \mu - gX^2 - 3gY^2 - 2hXY \end{pmatrix}$$

To simplify the calculations, **$g = 1$ and $h = 0$** will be considered, such that the system becomes:

$$\dot{Z} = \mu Z + i\Delta Z - Z|Z|^2 + F \qquad (6)$$

The expression for finding the fixed points becomes:

$$R^6 - 2\mu R^4 + (\mu^2 + \Delta^2)R^2 - F^2 = 0$$

And the Jacobian:

$$J(x,y) = \begin{pmatrix} \mu - 3X^2 - Y^2 & -\Delta - 2XY \\ \Delta - 2XY & \mu - X^2 - 3Y^2 \end{pmatrix}$$

This latter can also be written in polar coordinates from the system (4):

$$J(R,\theta) = \begin{pmatrix} \mu - 3R^2 & -Fsin\theta \\ \frac{Fsin\theta}{R^2} & \frac{-Fcos\theta}{R} \end{pmatrix}$$

At fixed points, using (5), the Jacobian depends only on R and not on θ :

$$J(R^*,\theta^*) = \begin{pmatrix} \mu - 3R^{*2} & -\Delta R^* \\ \frac{\Delta}{R^*} & \mu - R^{*2} \end{pmatrix}$$

The trace and determinant of the Jacobian at the fixed points are given by:

$$\mathrm{Tr}\big(J(R^*,\theta^*)\big) = 2\mu - 4R^{*2} \qquad (7)$$
$$\det(J(R^*,\theta^*)) = 3R^{*4} - 4\mu R^{*2} + \mu^2 + \Delta^2$$

These relationships allow to analyse the stability of the fixed points.

When $\Delta = 0.1$, $F = 0.3$ and $\mu = 1$, we observe in Figure 8 that there are three fixed points: one stable $(\det(J) > 0, \mathrm{Tr}(J) < 0, \mathrm{Tr}(J) - 4\,(\det J)^2 > 0)$, one unstable $(\det(J) > 0,\ \mathrm{Tr}(J) > 0, \mathrm{Tr}(J) - 4\,(\det(J))^2 > 0)$, and one saddle node $(\det(J) < 0)$. The stability of the fixed points is confirmed by the trend of the vector field. Moreover, the representative trajectories converge all to the stable fixed point and there is no stable limit cycle since the Poincaré-Bendixon's theorem is not verified as there is no closed region containing the unstable fixed point with the field vector pointing inside the region.

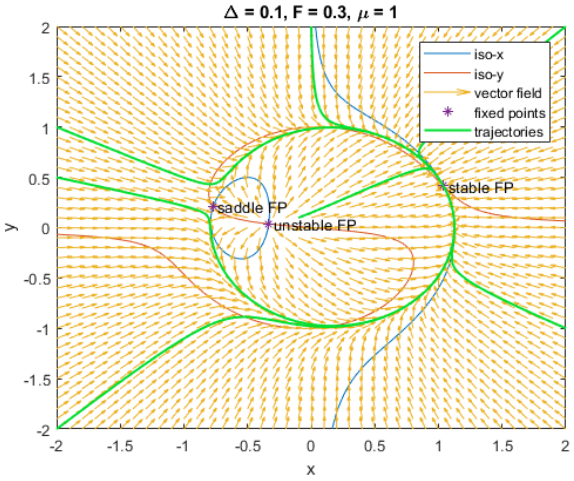

Figure 8 – Phase portrait of the system including isoclines, vector field, fixed points and representative trajectories. All trajectories converge to the stable fixed point and there is no limit cycle.

When $\Delta = 0.2$, $F = 0.6$ and $\mu = 1$, we observe in Figure 9 that there is only one fixed point which is stable. All trajectories converge to this fixed point and there is no stable limit cycle since there is no unstable fixed point as Poincaré-Bendixon's theorem requires. Moreover, as the system has a stable fixed point, the oscillator is synchronized by the external stimulus F.

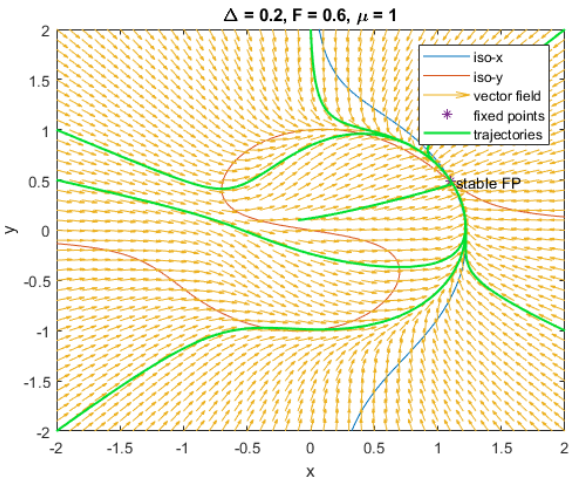

Figure 9 - Phase portrait of the system including isoclines, vector field, fixed points and representative trajectories. All trajectories converge to the unique stable fixed point. Moreover, the oscillator is synchronized by the external stimulus F.

If another set of parameters was considered, such as $\Delta = 0.6$, $F = 0.2$ and $\mu = 1$, we observe in Figure 10 the presence of an unstable spiral $(\det(J) > 0, \mathrm{Tr}(J) > 0,\ \mathrm{Tr}(J) - 4\,(\det(J))^2 < 0)$. Moreover, the Poincaré-Bendixon's theorem is verified as a region Γ can be drawn such that it contains the unstable spiral and such that the field vector points inward the region. All trajectories converge thus to this stable limit cycle.

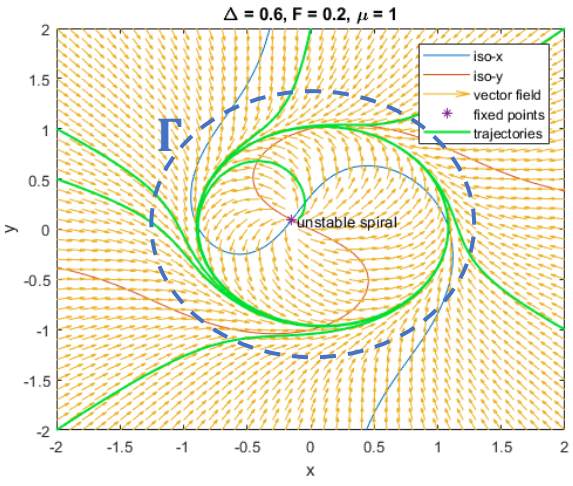

Figure 10 - Phase portrait of the system including isoclines, vector field, fixed points and representative trajectories. The unique fixed point is an unstable spiral. Poincaré-Bendixon's theorem is verified so a stable limit cycle is observable.

Explore the bifurcations

The previous figures show that the values of the angular frequency difference Δ and the amplitude of the perturbation F influence the presence or not of a limit cycle as well as synchronisation. Therefore, the influence of the two parameters Δ and F will be studied more deeply.

Firstly, phase portraits with F increasing from 0 to 1 with Δ fixed are represented in the attached files: "q19.gif" with $\Delta = 0.2$ and "q20.gif" with $\Delta = 0.4$.

When Δ is fixed to 0.2, we observe that at the beginning ($F = 0$), an unstable spiral is present leading to a limit cycle then, when F increases and becomes higher than around 0.2, two additional fixed points appear: a saddle fixed point and a stable fixed point. There is no limit cycle anymore and all trajectories converge to the stable fixed point. The system is thus synchronized. Then, beyond a value of F between 0.4 and 0.5, the saddle fixed point and the unstable spiral disappear and only the stable fixed point remains to which all trajectories converge.

When Δ remains constant at 0.4, a similar trend is observed except that the limit values of F for which the system behaves differently are different.

Similarly, the value of F can be fixed and the influence of the angular frequency difference Δ can be studied. Animated figures with F fixed and Δ varying between -0.8 and 0.8 can be found in the attached files: "q21.gif" with $F = 0.2$ and "q22.gif" with $F = 0.5$.

When F is set to 0.2, an unstable spiral is observed, and consequently a stable limit cycle for Δ from -0.8 until ~ -0.35. Then, there are three fixed points: one saddle fixed point, one unstable spiral and one stable fixed point for Δ from approximately -0.35 to -0.05 and from 0.05 to 0.35. The oscillator is synchronized in these intervals. Around 0, the unstable spiral is replaced by an unstable fixed point. Finally, above 0.35, there is only one unstable spiral and thus a stable limit cycle. A symmetric behaviour for opposite values of Δ is observed.

When F is equal to 0.5, although we observe also an unstable spiral for $|\Delta| >\sim 0.55$, there is now a unique stable fixed point for values of $|\Delta|$ under ~ 0.55. In this interval, the system is synchronized.

Arnold Tongues

The previous section shows that the dynamics of the system changes particularly based on the values of Δ and F. We can summarize the types of phase portrait in (Δ, F) planes called Arnold Tongues.

Figure 11 shows the number of fixed points depending on the values of Δ and F. We observe that generally, one fixed point is present except for a "triangular" region around $\Delta = 0$ and for $F < 0.5$ where the system has 3 fixed points.

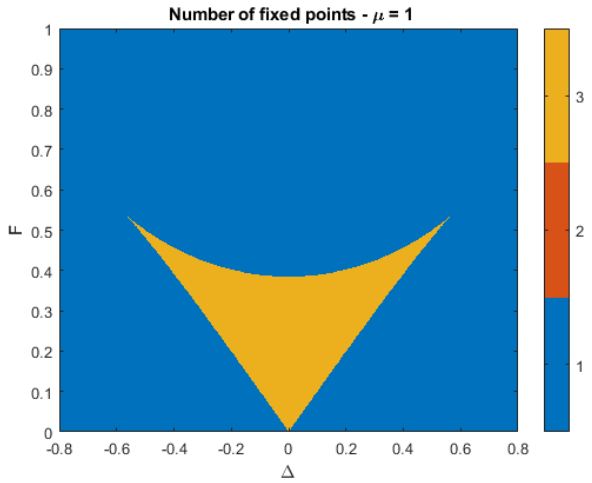

Figure 11 – Number of fixed points of the system depending on the values of Δ and F. For most of the couples, one fixed point is present except for a 'triangular' region around $\Delta = 0$ and for $F < 0.5$ where the system has 3 fixed points.

As defined previously, the system is said synchronized when it contains a stable fixed point or a stable spiral. In this case, the difference in phases between the two oscillators tends to be constant. Figure 12 shows the regions where the oscillator is synchronized by the external stimulus F. There is phase locking when the amplitude of the stimulus F is high ($F > 0.67$) regardless the angular frequency difference Δ or when the frequency of the oscillator and of the external signal are relatively close ($\Delta \approx 0$).

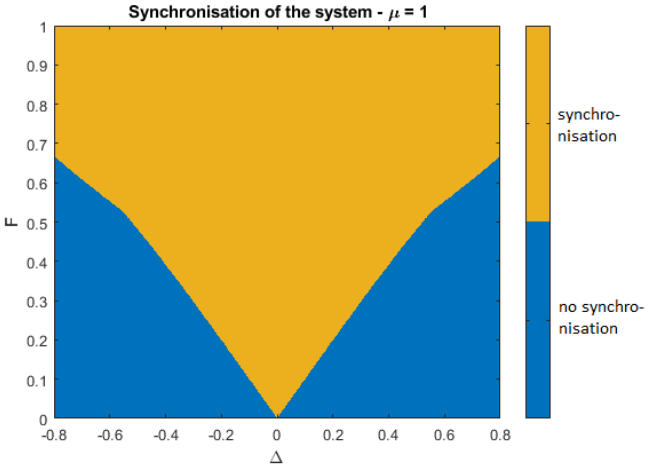

Figure 12 – Synchronisation or not of the system depending on the values of Δ and F. The oscillator is synchronized by the external stimulus F when the system has a stable fixed point or a stable spiral.

The regions can be analysed more deeply by looking at the types of fixed points as represented in Figure 13. The synchronisation region is mainly divided in 3 sub-regions: a dark blue region where there is a

unique stable fixed point and the dark and light green regions where three fixed points are coexisting, a stable fixed point, a saddle fixed point and either an unstable fixed point, or an unstable spiral. The no-synchronisation region corresponds to the presence of an unstable spiral. Moreover, we observe a symmetry for positive et negative values of Δ.

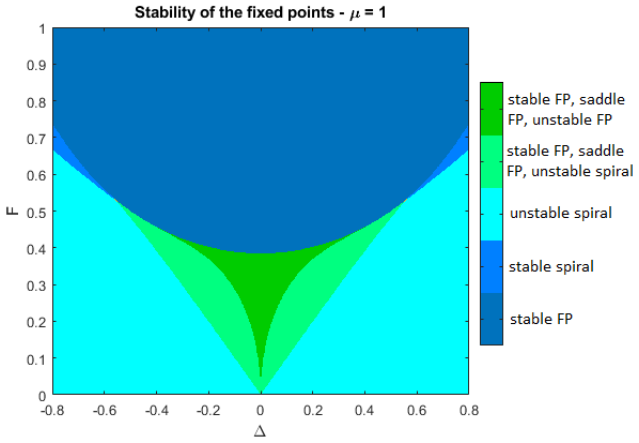

Figure 13 – Different combinations of fixed points depending on the values of Δ and F.

When varying the value of μ, we obtain different regions as depicted in Figure 14, 15 and 16. We can see that when μ is smaller, the region where there are three fixed points decreases whereas the synchronisation region increases.

When $\Delta \approx 0$, the angular frequency of the oscillator and of the external stimulus are almost similar. This leads to the fast entrainment of the oscillator. In contrast, when |Δ| becomes higher, the entrainment is slower. This corresponds to values at the extremity of the "tongue". In the case of fast entrainments, the oscillator is said "rigid" while it is said "sloppy" when the entrainment is slow.

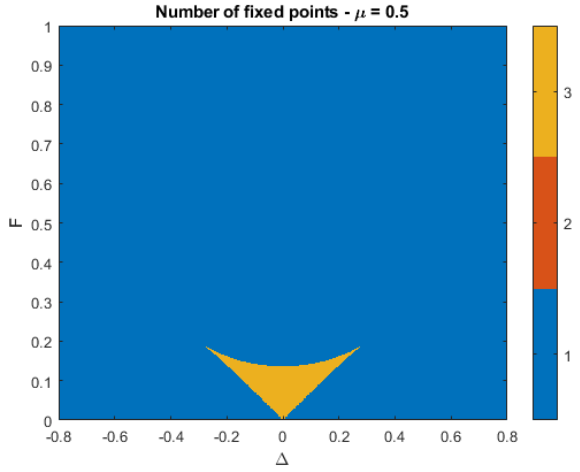

Figure 14 - Number of fixed points of the system for $\mu = 0.5$. The region with 3 fixed points is reduced and localized as a triangular around $\Delta = 0$.

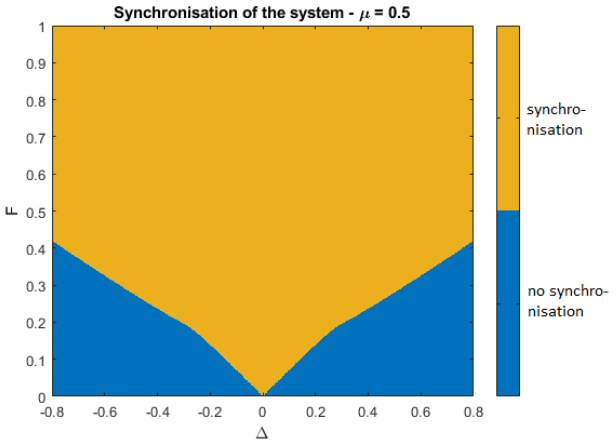

Figure 15 – Synchronisation or not of the system depending on the values of Δ and F with $\mu = 0.5$. The synchronisation region is larger when μ decreases.

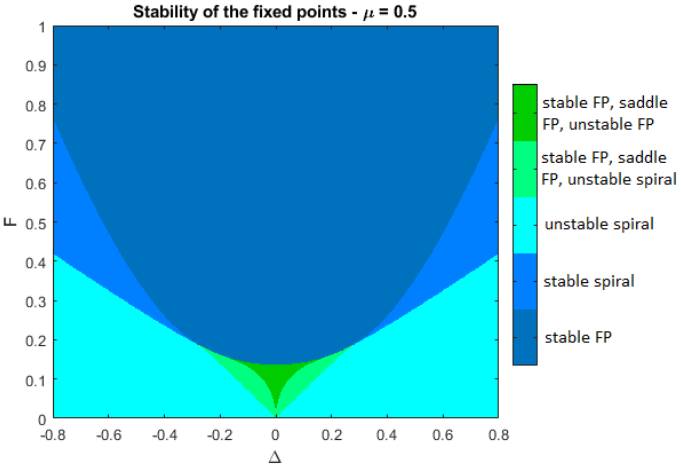

Figure 16 - Different combinations of fixed points depending on the values of Δ and F for $\mu = 0.5$.

Another point of interest could be the analysis of the entrained phase θ of the model ($Z = Re^{i\theta}$) in function of the angular frequency difference Δ for different values of μ and of the stimulus amplitude F. Indeed, after applying a perturbation, the oscillator becomes phase shifted. Considering absolute values, we observe in Figure 17 that smaller values of μ lead to smaller entrained phases. So, when μ is small, we have not only a larger synchronized region (see Figure 15) but also smaller entrained phases.

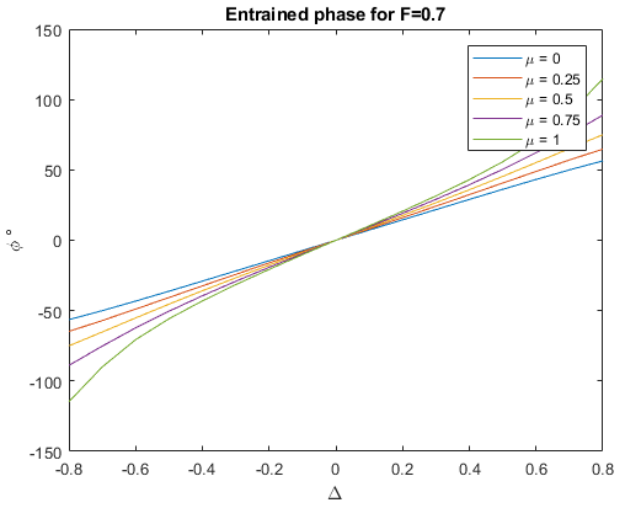

Figure 17 – Entrained phase in function of Δ for fixed $F = 0.7$ and different values of μ.

Concerning the stimulus amplitude F, Figure 18 shows that the higher the amplitude, the smaller the entrained phase (in absolute values).

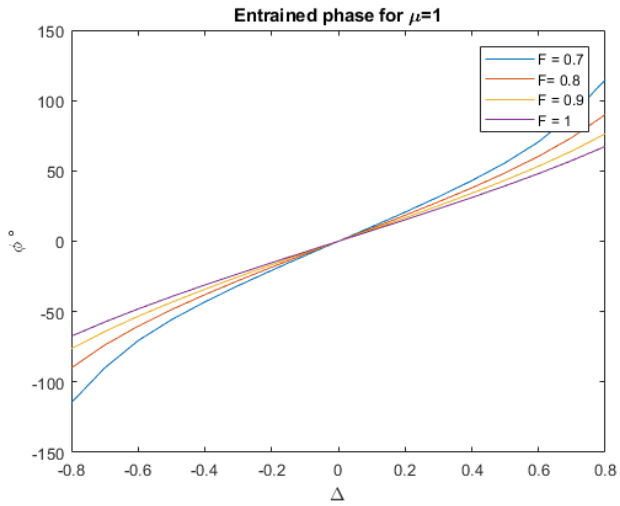

Figure 18 - Entrained phase in function of Δ for fixed $\mu = 1$ and different values of μ.

In other words, it can be said that, most of the time, a dephasing appears when the oscillator is perturbated. The phase shifting will be amplified if the angular frequency difference Δ is high, if μ is high or if stimulus amplitude F is low.

Most of the phase shifts are comprised between $-\pi/2$ and $\pi/2$. A negative value indicates a phase delay, whereas a positive value indicates a phase advance.

More bifurcations

Based on the system (6), we can say that the system will be stable if, at the fixed points, $\det(J) > 0$ and $\mathrm{Tr}(J) < 0$ (7). This means:

$$\begin{cases} 3R^4 - 4\mu R^2 + \mu^2 + \Delta^2 > 0 \\ R^2 > \dfrac{\mu}{2} \end{cases}$$

Therefore, every fixed point respecting $R^2 > \mu$ will always be stable.

In the following paragraph, Arnold Tongue diagrams will be studied with a nonzero value for h. We took $h = 0.2$ and base our discussion on Figure 19 , Figure 20 and Figure 21. We observe that the regions are not symmetrical anymore around $\Delta = 0$. However, for small values of the stimulus F, the synchronisation region is symmetrical around $\Delta = 0.2$, that is $\Delta = h$. So, the value of h seems to influence the position of the synchronized region around the angular frequency difference Δ.

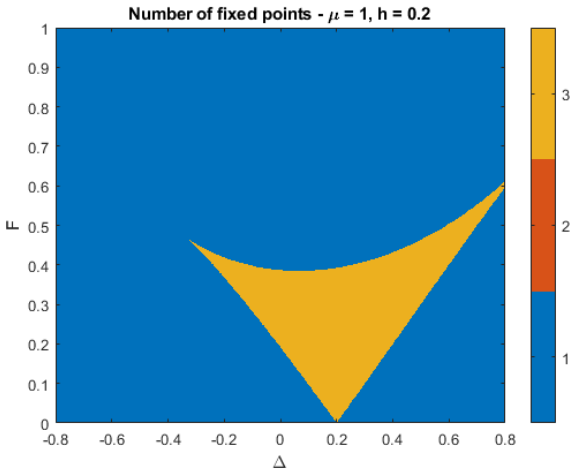

Figure 19 - Number of fixed points of the system for $h = 0.2$. The region with 3 fixed points is shifted to the right.

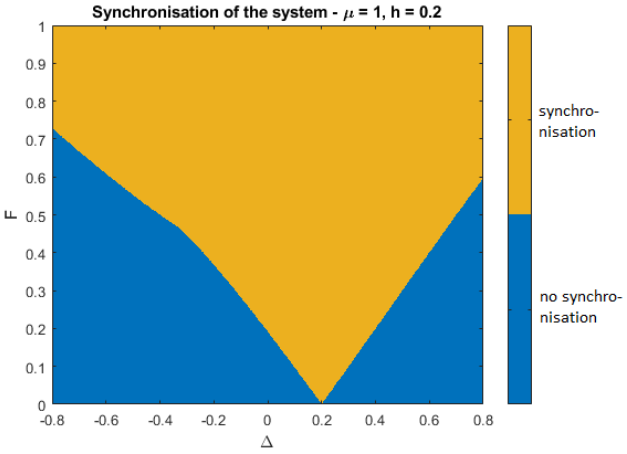

Figure 20 – Synchronisation or not of the system depending on the values of Δ and F with $h = 0.2$. The synchronisation region is shifted to the right when h increases.

In Figure 21, the bifurcation between the different regions will be analyse trough the red closed path starting from 1 in a counter clockwise direction.

Animated figures of the phase portrait corresponding to the path is provided in "more_bifucation.gif".

From 1 to 2, the oscillator has one unstable spiral located close to the origin and there is a limit cycle. The spiral moves to the left and becomes an unstable fixed point before the apparition of three fixed points. There is thus a small pink region containing one unstable fixed point. A limit cycle is still present in this region since the Poincaré-Bendixon's theorem is satisfied.

Then, in 3, the isoclines intersect three times and the path enters a region with three fixed points. The previous unstable fixed point remains but a stable fixed point and a saddle fixed point appear. There is no limit cycle anymore, but the oscillator is entrained as a stable fixed point is present.

The unstable fixed point is located near the origin and the two others are situated in negative y. As Δ grows, these two latter fixed points move away. Indeed, the isocline-x separates in a closed loop on the left and a curve on the right as shown in Figure 22. In 4, the unstable fixed point becomes an unstable spiral and in 5, it becomes again an unstable fixed point. The limit between a spiral and a fixed point is determined by the sign of $\mathrm{Tr}(J) - 4\,(\det(J))^2$ evaluated at the fixed point.

In 6, the closed loop whose size was reducing, disappears. Therefore, the number of fixed points changes from three to one. The remaining fixed point is stable.

From 6 to 7, this stable fixed point travels a big region before becoming a stable spiral (X has a negative value). All trajectories turn before converging to the spiral. The spiral becomes unstable in 8 and a limit cycle appears. From 8 to 1, the cycle grows to find back the configuration in 1 where the limit cycle is the biggest.

In conclusion, we can say that the bifurcations are not "abrupt" in the sense that the nature of the points are partially kept. At 2, the spiral becomes a fixed point but the instability is kept; at 3, the unstable fixed point remains; at 4 and 5, the unstable fixed point changes to a spiral and vice versa; at 6, the stable fixed point remains; at 7, it becomes a spiral but is still stable and at 8, the spiral becomes unstable. These characteristics are summarized in Table 1.

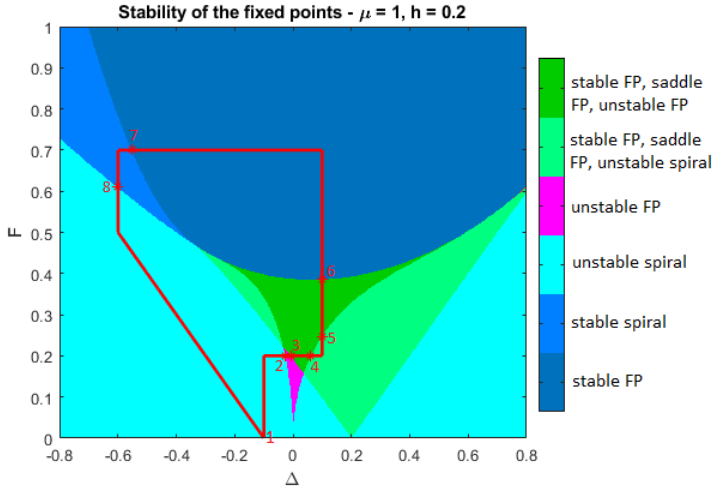

Figure 21 – Different combinations of fixed points depending on the values of Δ and F for $h = 0.2$. A new pink region (one unstable fixed point) appears close to $\Delta = 0$ for small values of F. The bifurcations between the regions is analysed through the closed red path.

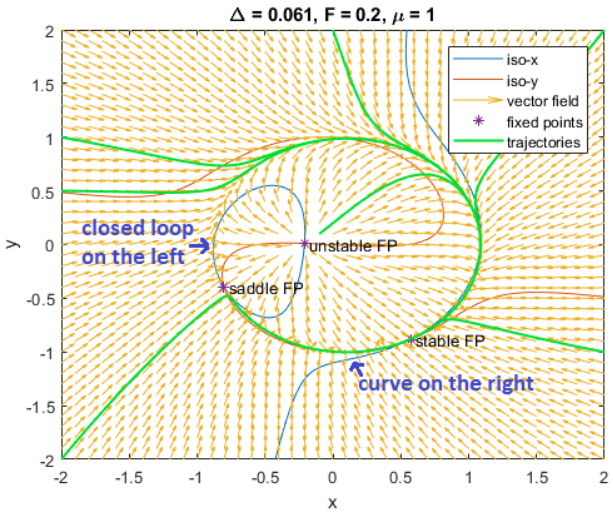

Figure 22 – Portrait phase of the oscillator at the left of the bifurcation 4. The isocline-x is divided in a closed loop in negative x on the left and a curve on the right.

1-2	1 Unstable spiral
2-3	1 Unstable fixed point
3-4	1 Unstable FP, 1 saddle FP, 1 stable FP
4-5	1 Unstable spiral, 1 saddle FP, 1 stable FP
5-6	1 Unstable FP, 1 saddle FP, 1 stable FP
6-7	1 stable FP
7-8	1 stable spiral
8-1	1 unstable spiral

Table 1 – Bifurcations between regions based on the red path in Figure 21. The bifurcations are smooth meaning that at least one characteristic from the previous region is kept (coloured or underlined).

Conclusion

In this report, a three-variable model was first analysed as circadian oscillations in single cells. Then, a generic 2D model of biological oscillators was studied near the onset of a stable limit cycle, called a supercritical Hopf bifurcation. Finally, the influence of different parameters was examined to understand the behaviour of the oscillator.

Appendix

.gif files and MATLAB scripts can be found in https://drive.google.com/drive/folders/1ok5LCruYINVJbL28MUbEnOopdOxocL7d?usp=sharing

References

- DIBNER, C., SCHIBLER, U., ALBRECHT, U. *The mammalian circadian timing system: organization and coordination of central and peripheral clocks*, Annual Review of Physiology, 2010.
- AGUILAR-ROBLERO, R. *Mechanisms of Circadian Systems in Animals and Their Clinical Relevance*, 2014
- ROENNEBERG, T. *The human circadian clock entrains to sun time*, Current Biology, 2007
- HARDIN, P., HALL, JC. and ROSBASH, M. *Feedback of the Drosophila period gene product on circadian cycling of its messenger RNA levels*, Nature 1990
- GONZE, D. *Coupling, entrainment, and synchronization of biological oscillator*. http://homepages.ulb.ac.be/~dgonze/TEACHING/synchro.pdf
- Ishida N, Kaneko M, Allada R (August 1999). "Biological clocks".